THE JOURNAL OF PHYSICAL CHEMISTRY C
A JOURNAL OF THE AMERICAN CHEMICAL SOCIETY

pubs.acs.org/JPCC

Article

In Situ Transmission Electron Microscopy of Disorder−Order Transition in Epitaxially Stabilized $FeGe_2$

Markus Terker,* Lars Nicolai, Samuel Gaucher, Jens Herfort, and Achim Trampert

Cite This: *J. Phys. Chem. C* 2021, 125, 2779−2784

Read Online

ACCESS | Metrics & More | Article Recommendations

ABSTRACT: Isothermal crystallization of amorphous Ge deposited on a cubic Fe_3Si/GaAs(001) substrate is performed by *in situ* annealing within a transmission electron microscope. It was found that the formation of epitaxially aligned tetragonal $FeGe_2$ is associated with a disorder−order phase transition mainly consisting of a rearrangement of the Fe/vacancy sublattice from a random distribution to alternating filled and empty layers. Additionally, atomically resolved high-angle annular dark-field scanning transmission electron microscopy and energy-dispersive X-ray spectroscopy demonstrated that the vertical lattice spacing of the Ge sublattice reduces across vacancy layers, indicating that strain minimization plays a role in the phase transition process. Crystallization and ordering are both found to proceed layer-by-layer and with square-root-shaped kinetics with a smaller transition rate for the latter.

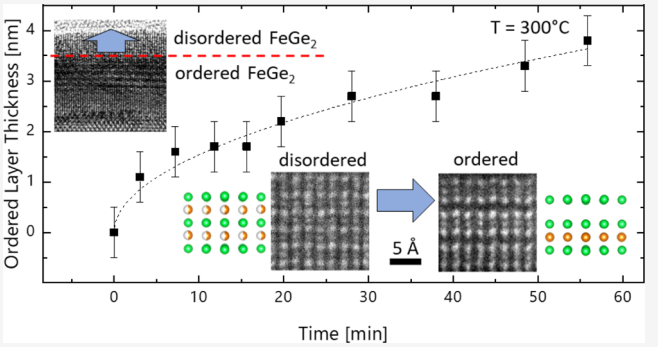

INTRODUCTION

Heterostructural interfaces can stabilize metastable crystalline structures by means of epitaxial constraints.[1−8] These heterostructures then often show different mechanical,[7] magnetic,[6,8] optical,[1,4,5] and transport properties,[1,6] which can be used to either optimize existing devices[1] or open up potential new applications.[6,8] Oftentimes, these strain stabilized structures are characterized by layered superstructures with layer orientation parallel to the interface along the growth direction.[6,8]

Another example has been observed in the case of solid-phase epitaxy of semiconducting Ge on ferromagnetic Fe_3Si.[9] For this nominally lattice matched cube-on-cube system, there is no influence of epitaxial strain and pure Ge is expected to form during solid-phase epitaxy. However, strong diffusion of Fe into the Ge film is detected at relatively low crystallization temperatures and, instead of pure Ge with a diamond structure, an epitaxial film with a Fe content of about 35% is obtained.[10] According to the Fe−Ge phase diagram in this composition range,[11] the formation of the stable $FeGe_2$ compound is expected with the tetragonal $CuAl_2$ crystal structure and space group $I4/mcm$.[12] X-ray and electron diffraction measurements together with high-angle annular dark-field (HAADF) scanning transmission electron microscopy (STEM) studies demonstrated, however, that a different metastable crystal structure has formed, which is characterized by a novel vacancy-ordered tetragonal $FeGe_2$ described by the $P4mm$ space group.[10]

In our earlier work, we used *in situ* high-resolution TEM (HRTEM) to observe the solid-phase epitaxy process inside the microscope. We have found that initial crystallization of the amorphous film does not immediately result in the mentioned ordered $FeGe_2$ structure but that there exists an intermediate state lacking the periodicity corresponding to the vacancy layers of the $P4mm$ phase.[13] A similar intermediate structure has been observed for the $FeSi_2$ alloy. This material too shows epitaxial crystal structures differing from the bulk phase.[14−18] In particular, the α-phase of $FeSi_2$ is interesting as it is comparable to the layered $FeGe_2$ structure.[19] While in bulk materials, this phase is only stable at above 920 °C, and it can also be observed at room temperature (RT) when stabilized by a Si substrate.[14,16,17] Further, for epitaxial systems, there exists a metastable cubic phase with a CsCl structure and an occupation of Fe sites of 50%. When annealed, this structure then transforms to the α- or the β-phase, which are also observed in bulk materials.[14,17] From this, it can be deduced that $FeGe_2$ forms a comparable phase with random occupation of the Fe/vacancy sublattice.

Received: November 30, 2020
Revised: January 6, 2021
Published: January 25, 2021

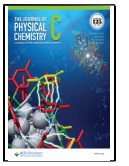

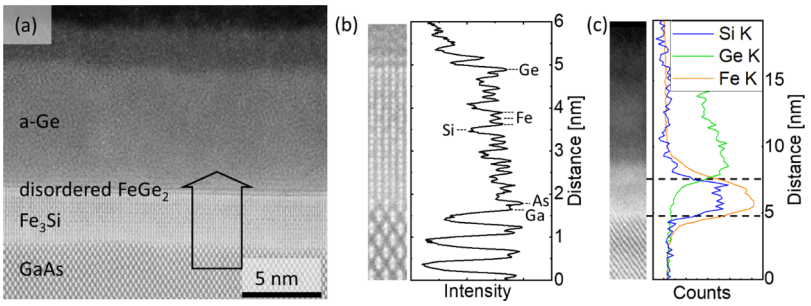

Figure 1. (a) HAADF STEM image of the sample before annealing. A 7−8 nm thick film of amorphous Ge is visible atop 3 nm of Fe_3Si. At the interface region, a thin film of disordered $FeGe_2$ has already formed. (b) Integrated line scan along the black arrow, including only every 2nd atomic plane. A magnified section of the image in (a) is depicted to the left. (c) EDX line scan showing the distribution of Fe, Ge, and Si across the interfaces.

In this work, we present our *in situ* TEM study of the disorder−order transition of $FeGe_2$ to shed light on the underlying strain and atomic diffusion-driven processes during solid-phase epitaxy. The pre- and post-annealing states are investigated with atomic resolution HAADF STEM and energy-dispersive X-ray spectroscopy (EDX) to define the initial and final structure in detail.

EXPERIMENTAL SECTION

For the present study, samples were prepared in a molecular beam epitaxy (MBE) chamber. First, a 3 nm thin cubic Fe_3Si film is epitaxially grown on the GaAs (001) substrate. Last, an amorphous (a-) Ge film with nominal 12 nm thickness is deposited at RT inside the same growth chamber.[20] Cross-sectional specimens for *in situ* TEM investigations were then prepared using a hybrid approach as described in a previous work.[13] In short, for this preparation technique, the sample is first conventionally prepared by mechanical grinding, dimpling and Ar^+ ion milling. Afterward, a focused ion-beam (FIB) device is utilized to cut out a thin part of the specimen and transfer it to a MEMS *in situ* heating chip. This avoids the common lamella preparation by FIB, which generally causes surface damage to the TEM sample.[21] The *in situ* TEM investigations were performed with a JEOL 2100F field emission microscope operating at an accelerating voltage of 200 kV. A double-tilt DENSSolutions Lightning D9+ holder is applied with commercial Wildfire MEMS chips for temperature control during the *in situ* TEM experiments. Before and after annealing, samples were additionally investigated by STEM and EDX spectroscopy in a C_s-aberration-corrected Jeol ARM 200F microscope operating at 200 kV. The experiments were performed in a dark-field scanning mode with a beam convergence acceptance angle of 68−280 mrad mainly generating Z-contrast imaging conditions.

The *in situ* heating experiments were conducted by ramping up the temperature from RT to 300 °C within 60 s and holding it there for 60 min before cooling down to RT again for 60 s.

RESULTS AND DISCUSSION

Characterization of the Initial Structure. The initial structure of the cross-sectional as-grown sample before annealing is observed by atomically resolved HAADF STEM, as depicted in Figure 1a. In this imaging mode, the contrast is mainly determined by the atomic number and the local thickness of the sample,[22,23] enabling the discrimination of the different material layers. Moreover, the crystalline material observed along a zone axis results in a brighter contrast compared to the corresponding amorphous material due to the channeling effect.[24] These imaging properties make it possible to clearly distinguish the different compositions, structures, and phases in the observed heterostructure.

In this regard, the lower part of Figure 1a shows the GaAs wafer along the ⟨110⟩ zone axis, and the bright material in the center corresponds to the epitaxially aligned Fe_3Si quasi substrate, and on top, the relatively dark area without appearance of periodic lattice planes or crystalline nanoclusters belongs to the a-Ge film. Fe_3Si has the expected thickness of 3 nm and forms a coherent and morphologically abrupt interface to the GaAs substrate including double atomic steps. Further, the center of the Fe_3Si film reflects the characteristic ordered DO_3 structure with darker spots for Si columns and a brighter one for the heavier Fe.[25] Toward the upper and lower interfaces, the DO_3 ordering becomes imperfect, and the crystal structure changes to the less ordered B2-type, indicating a disturbance in the ordering that is possibly caused by Fe interdiffusion and vacancy generation.

The a-Ge film has a thickness of 7−8 nm, which is smaller than the nominal value. It is remarkable that a thin layer of already crystallized material is visible at the interface to the Fe_3Si. The exact structure of this partially crystallized part of the film could not be determined due to the large remaining disorder. Figure 1b shows an intensity line scan across the interface at the location of the black arrow integrated over 20 atomic columns in combination with a magnified image of that area. For the integration, only every second atomic plane is considered to get a result that resembles a line scan across a single atom row but with improved signal-to-noise ratio. Here, each atom column can be clearly resolved as a separate peak with an intensity dependent on the mass-thickness. The overall intensity slope across the Fe_3Si layer stems from thickness variations of the TEM sample, but still the atom columns containing Si, Fe, or a mix thereof at the interface regions can be clearly distinguished (note the clear difference in contrast between the Si and the Fe columns in the center of Fe_3Si). Atop Fe_3Si, there is a continuous bright atomic layer with a HAADF STEM intensity indicative for pure Ge (contrast difference to Fe is similar to that between Fe and As on other interface), and some more faint atomic planes are visible on top with a spacing of 2.5−3.5 Å. The EDX line scan in Figure 1c shows the distribution of Fe, Si, and Ge along the heterostructure. The black dashed lines indicate the location of the original interfaces. In comparison to Si, Fe shows a strong out-diffusion from the Fe_3Si film. Especially toward the crystallized part of the Ge-film (recognizable here from the

https://doi.org/10.1021/acs.jpcc.0c10716
J. Phys. Chem. C 2021, 125, 2779−2784

bright contrast in the HAADF STEM to the left of the EDX line scan), there is a significant amount of Fe. Apart from that, no Fe signal is detectable in the still completely amorphous part of the Ge. It can therefore be assumed to still be pure a-Ge.

Crystallization and Disorder–Order Transition. In order to initiate the crystallization and ordering process, the sample is heated from RT to 300 °C within 1 min and kept at this temperature. Figure 2a summarizes a sequence of HRTEM

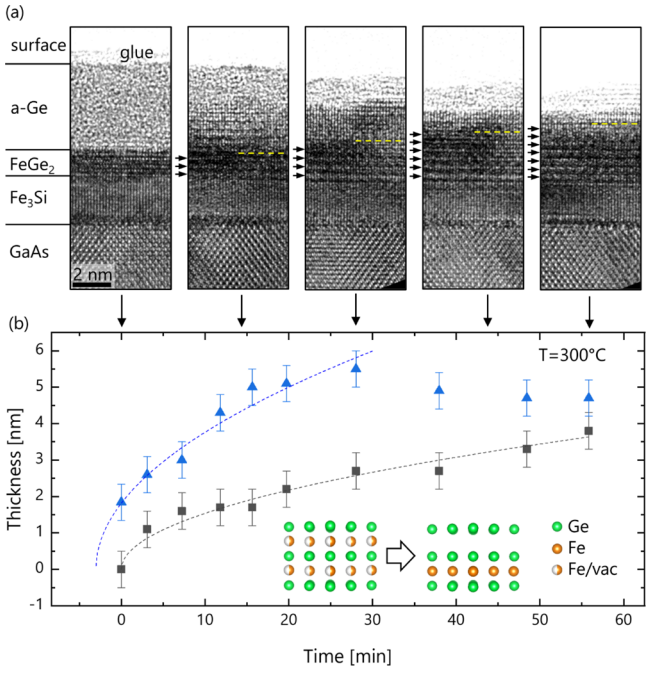

Figure 2. (a) Depicted images show snapshots of an *in situ* annealing experiment at 300 °C. Image after just reaching the target temperature, after 15 min, after 30 min, after 45 min, and after 60 min at 300 °C. The yellow dashed line indicates the transformation front of the vacancy ordering and black arrows indicate the periodic layers. (b) The thickness of the different transformed layers in the center of the images is plotted against annealing time. Models showing the atomic structure of the disordered and ordered phase are depicted as inset in the plot.

images of this isothermal annealing experiment taken at different times between 0 and 60 min after reaching the target temperature. At the beginning of the *in situ* recording directly after reaching 300 °C, a thin $FeGe_2$ layer has already crystallized at the Ge/Fe_3Si interface, while the rest of Ge is still in the amorphous state. This means that a heterogeneous nucleation has taken place whereby the crystallized region appears as thin, coherently grown epitaxial layer, with the crystal structure showing no sign of the vacancy-ordered $FeGe_2$ phase.

After 15 min of annealing, a large part of the Ge film has transformed to the crystalline disordered $FeGe_2$ phase. At the same time, in the preexisting $FeGe_2$ film near the interface to Fe_3Si, the occurrence of a periodic modulation in the HRTEM contrast becomes visible (indicated by short black arrows in Figure 2a), which is characteristic for the emergence of the vacancy-ordered $FeGe_2$ structure.[13] HAADF STEM images of both phases are depicted in Figure 3. Due to the Z-contrast and the much smaller surface sensitivity of HAADF STEM compared to HRTEM, the ordered structure of the film

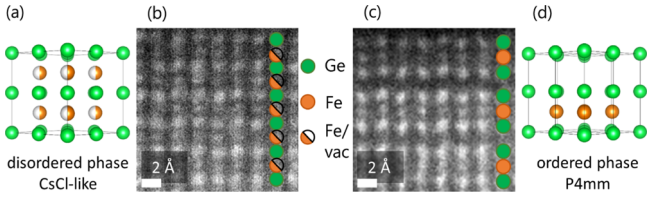

Figure 3. HAADF STEM images of the (b) disordered and (c) vacancy-ordered structure of $FeGe_2$ observed in the [110] direction. Colored dots indicate the atomic stacking order. Atomic models of the (a) disordered and (d) ordered phase of $FeGe_2$ observed in the [110] direction.

becomes clearly visible and the Fe/vacancy ordering can be clearly distinguished by means of the periodically arranged dark line contrast.

Within the next 15 min, the amorphous film has completely crystallized. The remaining amorphous material near the surface results from the epoxy adhesive. The ordered area of the $FeGe_2$ layer has also slowly expanded further in a layer-by-layer-like manner. During the next 30 min, this process continues until nearly the entire $FeGe_2$ film is in the ordered phase. The transformation front is marked by yellow dashed lines in Figure 2a. The layer-by-layer nature of this disorder–order transition indicates a higher in-plane than out-of-plane transformation rate.

Figure 2b summarizes the results of the kinetics of the amorphous-crystalline (blue triangles) as well as the disorder–order phase transformations (black squares) by plotting the thickness of the respective newly formed phases as a function of time. In agreement to our previous observation,[13] the crystallization kinetics can be described by a square root time behavior with high growth rate at the start. After about 30 min, the amorphous phase is almost exhausted, and the thickness of the crystallized layer remains constant. The small reduction in thickness after around 30 min can be attributed to a rearrangement of the front morphology by flattening the sample surfaces toward extended (001) terraces.

There is a one unit cell reduction in thickness of Fe_3Si during the early crystallization of the a-Ge. This means that the $FeGe_2$ phase does grow not only into the a-Ge but also into the Fe_3Si quasi-substrate due to the interdiffusion of Fe and of Ge. As a consequence, an additional $FeGe_2$ layer is formed at the interface. The second phase transformation, however, is not obviously accompanied by a further Fe_3Si thickness reduction. Therefore, it can be concluded that no significant persistent diffusion of Fe into the crystallized film is necessary for the transition to the ordered structure. This fact is in agreement with the assumption that the disordered phase has already the $FeGe_2$ stoichiometry.

On the other hand, the kinetics of the disorder–order phase transformation show a much slower course compared to the crystallization, except for the start of the annealing where the precrystallized film rapidly changes to the ordered phase. This transition continues after the crystallization process has finished until only a few atomic layers without the ordered structure remain after 60 min.

Resulting Structure. After the *in situ* annealing experiment, that is, after cooling down to RT, the sample has been further analyzed using HAADF STEM, as shown in Figure 4a. Figure 4b shows a magnified section of $FeGe_2$ next to a crystal structure model to the left and an integrated line scan over the area indicated with a black arrow in Figure 4a. According to

https://doi.org/10.1021/acs.jpcc.0c10716
J. Phys. Chem. C 2021, 125, 2779–2784

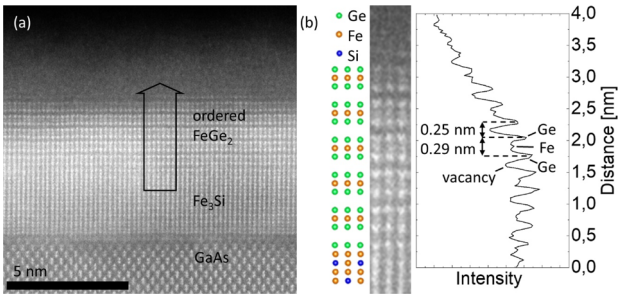

Figure 4. (a) HAADF STEM image of the TEM sample after in situ annealing. The vacancy-ordered structure of $FeGe_2$ is clearly visible. Green and orange dots on the left side of the image indicate the stacking of Fe and Ge. (b) Line scan across the interface at the location of the black arrow in (a) in front of a magnified image section. A magnified image section and a ball model of the ordered tetragonal structure are depicted on the left with green balls for Ge, orange for Fe, and blue for Si.

the layered tetragonal structure of $FeGe_2$, there is a periodic stacking sequence of Ge−Fe−Ge triple layers along the [001] direction, followed by a vacancy layer with larger spacing. The observed structure shows excellent agreement with the structural model of the ordered tetragonal $FeGe_2$ on the left side of the figure.[10] Additionally, the clearly distinguishable peaks in the line scan can be attributed to positions of Ge (Z = 32), Fe (Z = 26), and vacancies. This makes it possible to compare the lattice spacings of Ge layers across vacancy layers and layers filled with Fe atoms. Here, we measure 0.25 ± 0.01 nm in the former and 0.29 ± 0.01 nm in the latter case. This 0.04 ± 0.02 nm difference in lattice plane spacing between occupied and empty layers is slightly larger than the value reported in ref 10 by a bit more than the error margin. Possibly, this can be explained by a more complete ordering of the Fe/vacancy sublattice in the present sample.

The interface between Fe_3Si and $FeGe_2$ is not perfectly sharp due to interdiffusion, but along most of the interface, the Fe_3Si is capped with Ge followed by a vacancy layer and the ordered $FeGe_2$ (cf. model in Figure 4b). However, the first vacancy layer need not necessarily be completely emptied of Fe atoms, which can lead to shifts of half a unit cell in the stacking order (see Figure 5). Further, there are some locations, where the ordering of vacancies is disturbed, as depicted in Figure 5a, which shows a HAADF image that is Fourier filtered to make the vacancy ordering more directly visible. In the central part of the image, the ordering process does not seem to have occurred. Instead, Fe and vacancies randomly share the sublattice, as depicted in the atomic model at the top of Figure 5a. The difference between the center and the edges of the depicted section becomes apparent when looking at the intensity line scans along the red and blue arrow shown in Figure 5a. While the blue line again shows the three distinct intensity levels for vacancy, Fe and Ge atom columns the red line varies only between two intensities, that is, Ge and Fe/vacancy. Interestingly, these disordered sections reflect a bulging. This demonstrates that the observed second phase transition consists of more than just a rearrangement of the Fe atoms and the vacancies. Due to the ordering in the Fe/vacancy sublattice, the Ge lattice relaxes, respectively, from equidistant (001) planes with a spacing of 0.28 ± 0.01 to 0.25 ± 0.01 nm across vacancy layers and 0.29 ± 0.01 nm for Fe filled layers. This means that the spacing of two subsequent Ge-layers in the ordered structure is 0.02 nm smaller compared

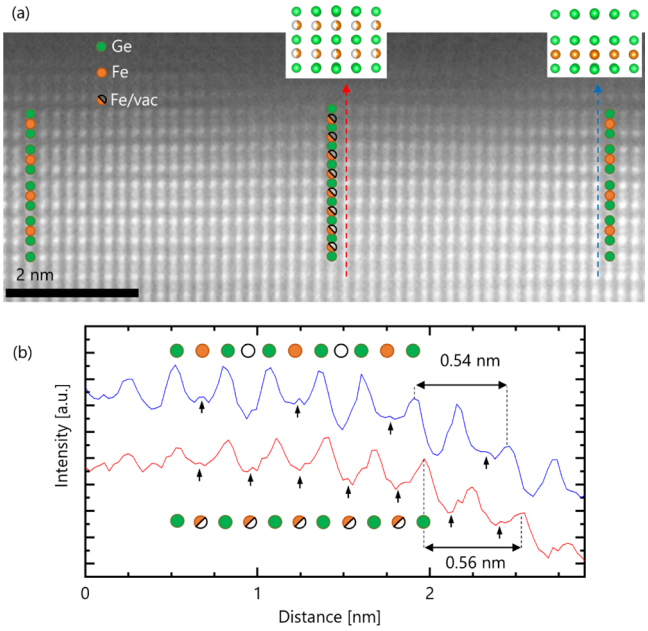

Figure 5. (a) Fourier filtered image, showing a small section of disordered $FeGe_2$ surrounded by the layered phase as indicated by green and orange dots. Structural models showing the two phases are shown as insets at the top. (b) Intensity line scans along the red and blue arrows in (a). Black arrows indicate the position of Fe peaks.

to two layers of the disordered one. Due to the coherent nature of the epitaxial interface, an effect on the in-plane lattice spacing is not observed. However, due to the expected larger lattice constant of the disordered crystal, the associated strain could stimulate the phase transition if that reduced the mismatch toward Fe_3Si. This would explain why the transformation starts at the interface. Further, the strain at the interface region between the ordered and disordered region could cause the much faster in-plane transformation rate, resulting in the layer-by-layer-like transition.

Stacking Mismatch Boundaries. As already mentioned before, there are some areas of the sample where there is Fe already in between the first two Ge layers, while most of the film starts with an empty layer after the first Ge. At the edge of two of those domains, this can lead to a stacking mismatch boundary (SMB) where the ordering between vacancy and Fe layers is shifted by half a unit cell. One example of a region with two closely spaced SMB is depicted in Figure 6a. It shows a HAADF STEM image of the sample after annealing inside the microscope. In the image, the position of vacancy layers is highlighted by small black arrows and the approximate location of the SMB is indicated with a red dashed line. To show this in more detail, a magnified view of the area is depicted in Figure 6b, marked with a black dashed line in (a). Here, the location of vacancy layers is again indicated by black arrows. Additionally, the stacking of Ge and Fe layers is also indicated by green and orange dots. Toward the sides of the image, the Fe and vacancy layers can clearly be distinguished, and the iron columns can be separately resolved. However, this is not the case in the center of the image, where the stacking order changes from one side to the other. This indicates that the SMB is probably inclined with respect to the viewing direction, and in the center, we see a projection through both domains.

This kind of defect is commonly observed in van der Waals bonded layered materials. A similar structure was observed for

https://doi.org/10.1021/acs.jpcc.0c10716
J. Phys. Chem. C 2021, 125, 2779−2784

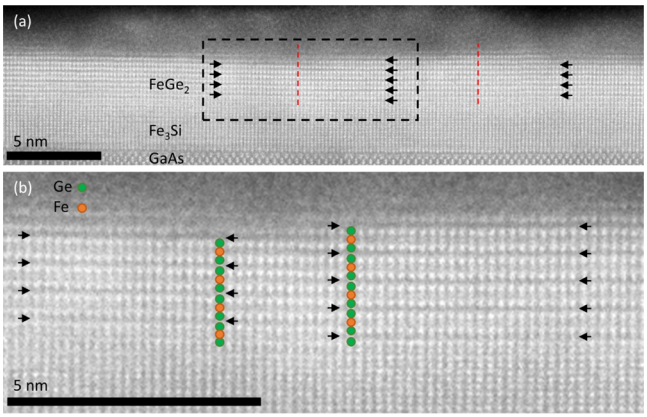

Figure 6. (a) HAADF STEM images of the sample after the annealing experiment presented in Figure 2. The black arrows indicate the position of vacancy layers which shift by half a unit cell at the red dashed lines, forming antiphase boundaries. (b) Magnified image of the section marked with a black dashed line in (a). Again, black arrows indicate vacancy layers. Additionally, the atomic order on both sides of the SMB is indicated by green and orange dots.

the bilayer defect in hexagonal Ge−Sb−Te-based materials.[26,27] However, in that case, this defect results from changes in the stacking order, while for $FeGe_2$, the step is generated at the interface to the substrate, and the atomic layering is only shifted by half a period across the boundary. Further, for $FeGe_2$, the defect repeats vertically at every vacancy layer making it two dimensional rather than a one dimensional.

Comparison to Annealing inside the MBE. Notably, the resultant ordered $FeGe_2$ structure obtained by the *in situ* TEM experiment is in excellent agreement with the structure observed after performing the annealing in the MBE chamber directly after deposition.[10] It can therefore be assumed that the diffusion processes during structure transformation observed *in situ* were not severely influenced by the specimen preparation. Especially, there seems to be little Ga implantation which is also confirmed by EDX analysis. Further, the additional surfaces do not change the strain state enough to prevent the stabilization of the *P4mm* structure of $FeGe_2$. However, it could be observed that the crystallization process proceeded faster in the sample regions exposed to the electron beam than in those which are not illuminated while at 300 °C. There are several possible ways in which the electron beam and the sample can interact.[28] In this case, most likely beam heating is the main contributor as it can explain the slower transformation rate without affecting the result. In total, the results underline the viability of the hybrid sample preparation approach for the high-resolution investigation of planar heterostructures.

CONCLUSIONS

We successfully applied *in situ* TEM to directly observe the disorder−order transition in the $FeGe_2$ alloy grown by solid-phase epitaxy on Fe_3Si. It could be shown that the a-Ge first crystallized to disordered $FeGe_2$ under the influence of Fe diffusion into the amorphous film and then transformed into the vacancy-ordered $FeGe_2$ phase with the *P4mm* space group. This transition was observed to start at the Fe_3Si interface and transform the material layer by layer from bottom up. The disorder−order transition was found to proceed much slower than the crystallization. Further, we observed that the disordered structure had a larger lattice spacing in growth direction, which confirms that strain could promote the phase transition. Comparison of the *in situ* TEM results with MBE-annealed samples demonstrates that the hybrid preparation approach yielded a high-quality sample with minimal contamination and surface damage. Therefore, this hybrid approach could help to apply *in situ* TEM to more atomic-level investigations of planar heterostructures.

AUTHOR INFORMATION

Corresponding Author

Markus Terker − *Paul-Drude-Institut für Festkörperelektronik, 10117 Berlin, Germany;* orcid.org/0000-0003-1793-6166; Phone: +49 (0)30 20377266; Email: terker@pdi-berlin.de

Authors

Lars Nicolai − *Paul-Drude-Institut für Festkörperelektronik, 10117 Berlin, Germany*

Samuel Gaucher − *Paul-Drude-Institut für Festkörperelektronik, 10117 Berlin, Germany*

Jens Herfort − *Paul-Drude-Institut für Festkörperelektronik, 10117 Berlin, Germany*

Achim Trampert − *Paul-Drude-Institut für Festkörperelektronik, 10117 Berlin, Germany;* orcid.org/0000-0001-7949-643X

Complete contact information is available at: https://pubs.acs.org/10.1021/acs.jpcc.0c10716

Notes

The authors declare no competing financial interest.

ACKNOWLEDGMENTS

The authors would like to thank M. Matzeck for the FIB sample preparation and M. Hanke for critical reviewing of the manuscript. Parts of this work have been funded by the European Union and the State of Berlin via the ERDF project 2016011843.

REFERENCES

(1) Chen, Y.; Lei, Y.; Li, Y.; Yu, Y.; Cai, J.; Chiu, M.-H.; Rao, R.; Gu, Y.; Wang, C.; Choi, W.; et al. Strain Engineering and Epitaxial Stabilization of Halide Perovskites. *Nature* **2020**, *577*, 209−215.

(2) Mäder, K. A.; von Känel, H.; Baldereschi, A. Electronic Structure and Bonding in Epitaxially Stabilized Cubic Iron Silicides. *Phys. Rev. B: Condens. Matter Mater. Phys.* **1993**, *48*, 4364−4372.

(3) Ourmazd, A.; Bean, J. C. Observation of Order-Disorder Transitions in Strained-Semiconductor Systems. *Phys. Rev. Lett.* **1985**, *55*, 765−768.

(4) Lee, S.; Freysoldt, C.; Neugebauer, J. Ordering Phenomena and Formation of Nanostructures in $In_xGa_{1-x}N$ Layers Coherently Grown on GaN(0001). *Phys. Rev. B: Condens. Matter Mater. Phys.* **2014**, *90*, 245301.

(5) Wegscheider, W.; Olajos, J.; Menczigar, U.; Dondl, W.; Abstreiter, G. Fabrication and Properties of Epitaxially Stabilized Ge / α-Sn Heterostructures on Ge(001). *J. Cryst. Growth* **1992**, *123*, 75−94.

(6) Jeen, H.; Choi, W. S.; Biegalski, M. D.; Folkman, C. M.; Tung, I.-C.; Fong, D. D.; Freeland, J. W.; Shin, D.; Ohta, H.; Chisholm, M. F.; Lee, H. N. Reversible Redox Reactions in an Epitaxially Stabilized $SrCoO_x$ Oxygen Sponge. *Nat. Mater.* **2013**, *12*, 1057−1063.

(7) Yashar, P. C.; Barnett, S. A.; Hultman, L.; Sproul, W. D. Deposition and Mechanical Properties of Polycrystalline Y_2O_3/ZrO_3 Superlattices. *J. Mater. Res.* **1999**, *14*, 3614−3622.

(8) Corbellini, L.; Lacroix, C.; Harnagea, C.; Korinek, A.; Botton, G. A.; Ménard, D.; Pignolet, A. Epitaxially Stabilized Thin Films of ϵ-Fe_2O_3 (001) Grown on YSZ (100). *Sci. Rep.* **2017**, *7*, 3712.
(9) Gaucher, S.; Jenichen, B.; Herfort, J. Ferromagnet/Semiconductor/Ferromagnet Hybrid Trilayers Grown Using Solid-Phase Epitaxy. *Semicond. Sci. Technol.* **2018**, *33*, 104005.
(10) Jenichen, B.; Hanke, M.; Gaucher, S.; Trampert, A.; Herfort, J.; Kirmse, H.; Haas, B.; Willinger, E.; Huang, X.; Erwin, S. C. Ordered Structure of FeGe2 Formed during Solid-Phase Epitaxy. *Phys. Rev. Mater.* **2018**, *2*, 051402.
(11) Okamoto, H. Fe-Ge (Iron-Germanium). *J. Phase Equilibria Diffus.* **2008**, *29*, 292.
(12) Satya Murthy, N. S.; Begum, R. J.; Somanathan, C. S.; Murthy, M. R. L. N. Magnetic Structures in the Iron-Germanium System. *Solid State Commun.* **1965**, *3*, 113−116.
(13) Terker, M.; Jenichen, B.; Herfort, J.; Trampert, A. In Situ Transmission Electron Microscopy of Solid Phase Epitaxy of Ge on Fe_3Si. *Semicond. Sci. Technol.* **2019**, *34*, 124004.
(14) Lin, X. W.; Behar, M.; Desimoni, J.; Bernas, H.; Washburn, J.; Liliental-Weber, Z. Low-temperature Ion-induced Epitaxial Growth of A-$FeSi_2$ and Cubic $FeSi_2$ in Si. *Appl. Phys. Lett.* **1993**, *63*, 105−107.
(15) Miiller, W.; Tomczak, J. M.; Simonson, J. W.; Smith, G.; Kotliar, G.; Aronson, M. C. Protected Fe Valence in Quasi-Two-Dimensional α -$FeSi_2$. *J. Phys.: Condens. Matter* **2015**, *27*, 175601.
(16) Moroni, E. G.; Wolf, W.; Hafner, J.; Podloucky, R. Cohesive, Structural, and Electronic Properties of Fe-Si Compounds. *Phys. Rev. B: Condens. Matter Mater. Phys.* **1999**, *59*, 12860−12871.
(17) Jedrecy, N.; Waldhauer, A.; Sauvage-Simkin, M.; Pinchaux, R.; Zheng, Y. Structural Characterization of Epitaxial A-Derived $FeSi_2$ on Si(111). *Phys. Rev. B: Condens. Matter Mater. Phys.* **1994**, *49*, 4725−4730.
(18) Goldfarb, I.; Cesura, F.; Dascalu, M. Magnetic Binary Silicide Nanostructures. *Adv. Mater.* **2018**, *30*, 1800004.
(19) Villars, P.; Calvert, L. D. *Pearson's Handbook of Crystallographic Data for Intermediate Phases*; American Society for Metals: Cleveland, OH, 1985.
(20) Gaucher, S.; Jenichen, B.; Kalt, J.; Jahn, U.; Trampert, A.; Herfort, J. Growth of Fe_3Si/Ge/Fe_3Si Trilayers on GaAs(001) Using Solid-Phase Epitaxy. *Appl. Phys. Lett.* **2017**, *110*, 102103.
(21) Mayer, J.; Giannuzzi, L. A.; Kamino, T.; Michael, J. TEM Sample Preparation and FIB-Induced Damage. *MRS Bull.* **2007**, *32*, 400−407.
(22) Hartel, P.; Rose, H.; Dinges, C. Conditions and Reasons for Incoherent Imaging in STEM. *Ultramicroscopy* **1996**, *63*, 93−114.
(23) Pennycook, S. J. Seeing the Atoms More Clearly: STEM Imaging from the Crewe Era to Today. *Ultramicroscopy* **2012**, *123*, 28−37.
(24) Pennycook, S. J. Z-Contrast Stem for Materials Science. *Ultramicroscopy* **1989**, *30*, 58−69.
(25) Pennycook, S.; Jesson, D. High-Resolution Incoherent Imaging of Crystals. *Phys. Rev. Lett.* **1990**, *64*, 938−941.
(26) Lotnyk, A.; Ross, U.; Dankwort, T.; Hilmi, I.; Kienle, L.; Rauschenbach, B. Atomic Structure and Dynamic Reconfiguration of Layered Defects in van Der Waals Layered Ge-Sb-Te Based Materials. *Acta Mater.* **2017**, *141*, 92−96.
(27) Wang, J.-J.; Wang, J.; Du, H.; Lu, L.; Schmitz, P. C.; Reindl, J.; Mio, A. M.; Jia, C.-L.; Ma, E.; Mazzarello, R.; Wuttig, M.; Zhang, W. Genesis and Effects of Swapping Bilayers in Hexagonal $GeSb_2Te_4$. *Chem. Mater.* **2018**, *30*, 4770−4777.
(28) Egerton, R. F.; Li, P.; Malac, M. Radiation Damage in the TEM and SEM. *Micron* **2004**, *35*, 399−409.

NOTE ADDED AFTER ISSUE PUBLICATION

This article was initially published with an incorrect copyright statement and was corrected on or around May 5, 2021.

https://doi.org/10.1021/acs.jpcc.0c10716
J. Phys. Chem. C 2021, 125, 2779−2784